Polaronic correlations and phonon renormalization in L a1-x S rxMn O3 (x=0.2, 0.3)

Maschek, M.; Castellan, J. P.; Lamago, D.; Reznik, D.; Weber, F.

DOI
10.1103/PhysRevB.97.245139

Publication date
2018

Document Version
Final published version

Published in
Physical Review B

Polaronic correlations and phonon renormalization in $La_{1-x}Sr_xMnO_3$ ($x = 0.2, 0.3$)

M. Maschek,[1,2] J.-P. Castellan,[1,3] D. Lamago,[1,3] D. Reznik,[4] and F. Weber[1]

[1]*Institute for Solid State Physics, Karlsruhe Institute of Technology, D-76021 Karlsruhe, Germany*

[2]*Fundamental Aspects of Materials and Energy, Faculty of Applied Sciences, Delft University of Technology, Mekelweg 15, 2629 JB Delft, The Netherlands*

[3]*Laboratoire Léon Brillouin (CEA-CNRS), CEA-Saclay, F-91911 Gif-sur-Yvette, France*

[4]*Department of Physics, University of Colorado at Boulder, Boulder, Colorado 80309, USA*

(Received 6 October 2017; published 25 June 2018)

According to standard theory the magnetoresistance magnitude in ferromagnetic manganites crucially depends on the electron-phonon coupling strength. We showed that in $La_{0.7}Sr_{0.3}MnO_3$ the phonon renormalization is strong, despite its relatively small magnetoresistance. Here, we report results of a similar inelastic neutron-scattering investigation of a closely related compound, $La_{0.8}Sr_{0.2}MnO_3$, where the magnetoresistance is enhanced. We find similar phonon renormalization and dynamic CE-type polaron correlations as in $La_{0.7}Sr_{0.3}MnO_3$. However, quantitative comparison of the results for the two samples shows that only polaron lifetime is well correlated with the strength of the colossal magnetoresistance.

DOI: 10.1103/PhysRevB.97.245139

I. INTRODUCTION

The manganites have complex phase diagrams, due to strongly competing magnetic, orbital, charge, and lattice degrees of freedom [1]. This competition leads to a unique property in the ferromagnetic manganites known as colossal magnetoresistance (CMR) [2,3]. The CMR manganites exhibit a simultaneous transition from a ferromagnetic (FM) and metallic ground state to a paramagnetic (PM) insulating phase at elevated temperatures. An applied magnetic field stabilizes ferromagnetism and results in a strongly reduced resistivity at the zero-field Curie temperature T_C. In the insulating phase strong electron-lattice coupling via the Jahn-Teller (JT) [4] effect favors lattice distortions that trap the charge carriers. leading to the formation of polarons [5–7]. These polarons involve cooperative lattice distortions that correspond to short-range charge and orbital order (COO) of Mn^{3+} (JT-active) and Mn^{4+} (JT-inactive) ions [8,9]. In many manganites correlations of those polarons result in superstructures of the CE-type [10,11] on heating through T_C into the PM phase.

The CE-type short-range COO associated with the ordering wave vector $\boldsymbol{q}_{CE} \approx (1/4, 1/4, 0)$ [10] forms in prototypical CMR manganites such as $La_{0.7}Ca_{0.3}MnO_3$ [12] and $La_{1.2}Sr_{1.8}Mn_2O_7$ [13].

Magnitude of the magnetoresistance effect is expressed by $-[\rho(B) - \rho(0)]/\rho(0)$ [$\rho(B)$: resisitivity at magnetic field B]. Many CMR manganites have an inverse correlation between magnetoresistance magnitude and T_C: The smaller the T_C the bigger the resistivity jump on applying magnetic field [1]. Standard theory [5,6] links the absolute value of T_C directly to the relative strengths of the competing interactions: A low T_C indicates strong electron-phonon coupling (EPC), promoting JT distortions, whereas a high T_C points to weak EPC.

Here we focus on the FM manganites of the $La_{1-x}Sr_xMnO_3$ family having a rhombohedral structure below 750 K. The Curie temperatures in the Sr-doped system are among the highest of all FM manganites with $T_C = 350$ and 305 K for $x = 0.3$ and 0.2, respectively [14,15].

Previously we investigated $La_{0.7}Sr_{0.3}MnO_3$ [16], which had been considered to be a pure double-exchange system with minimal JT electron-lattice interaction. However, we found that this compound also features CE-type correlated polarons and strong electron-phonon renormalization. The polarons' correlations are short-range and dynamic [16], with a correlation length for the polaronic fluctuations of $\xi_{x=0.3} = 34(4)$ Å and the lifetime of 1.00(15) ps. Similar results have been reported by others [17].

The magnetoresistance at T_C in $La_{0.7}Sr_{0.3}MnO_3$ is 0.35 for $B = 15$ T. Here we focus on the slightly lower doped $La_{0.8}Sr_{0.2}MnO_3$ where the FM-PM transition is accompanied by a metal-insulator transition. This subtle difference in the phase transition is reflected in much stronger CMR, which is 0.75 for 15 T in $La_{0.8}Sr_{0.2}MnO_3$ [14]. This contrast should be reflected in its atomic lattice response (both in the phonons and the polaronic distortions) compared to that of $La_{0.7}Sr_{0.3}MnO_3$.

We performed inelastic neutron-scattering measurements of $La_{0.8}Sr_{0.2}MnO_3$ focusing on the evolution of the transverse acoustic (TA) phonon mode propagating along the [110] direction and scattering from correlated polarons in the vicinity of T_C. Then we compared the results with our previous investigation of $La_{0.7}Sr_{0.3}MnO_3$ reported in Ref. [16].

II. EXPERIMENT

The sample was a high-quality single crystal of $La_{0.8}Sr_{0.2}MnO_3$ with a volume of about 0.7 cm^3. Inelastic neutron measurements were performed on the 1-T neutron triple-axis spectrometer at the ORPHEE reactor (LLB, CEA Saclay) using doubly focusing PG002 monochromator and analyzer crystals. The final energy was fixed to 14.7 meV. We performed energy scans at a constant-momentum-transfer $\boldsymbol{Q} = \boldsymbol{\tau} + \boldsymbol{q}$, where $\boldsymbol{\tau}$ and $\boldsymbol{q}$ are reciprocal lattice vector and reduced momentum transfer, respectively. The experimental resolution was obtained from standard calculations using the RESCAL program package [18]. In our work on $La_{0.8}Sr_{0.2}MnO_3$

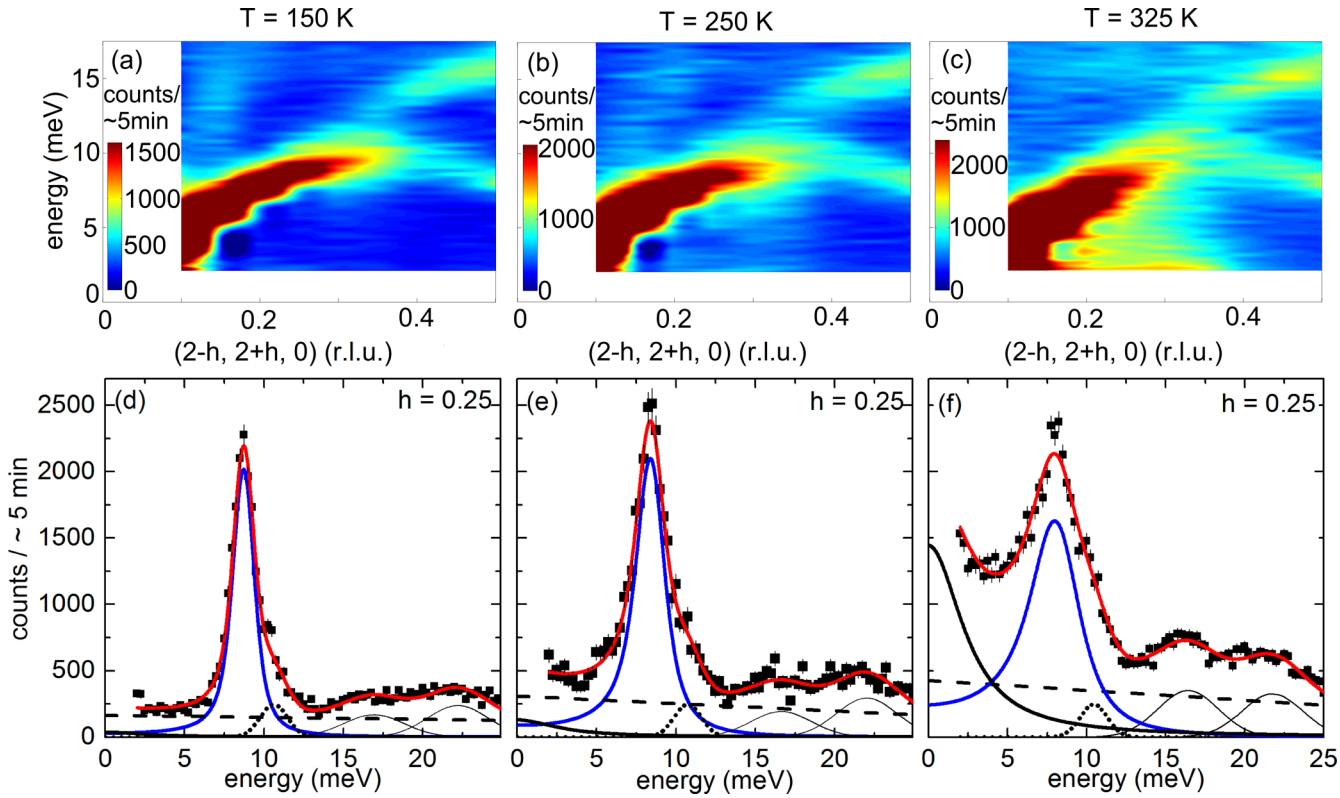

FIG. 1. (a)–(c) Color-coded contour maps representing inelastic neutron-scattering intensities along $\boldsymbol{Q} = (2-h, 2+h, 0)$, $0.1 \leqslant h \leqslant 0.5$ and energies $2\,\text{meV} \leqslant E \leqslant 17\,\text{meV}$. (d)–(f) Corresponding energy scans at $\boldsymbol{Q} = (1.75, 2.25, 0)$ for $T = 150\,\text{K}$ (d), 250 K (e), and 325 K (f). In (d)–(f), solid (red) lines are fits consisting of a damped harmonic oscillator function for the TA mode (solid and blue), a Lorentzian for quasielastic scattering (solid and black, see text), and the estimated background (dashed). The Gaussians (thin black lines) denote other modes and the dotted lines denote temperature-independent artifacts ($E \approx 10\,\text{meV}$).

we used the same experimental conditions as in our work on $La_{0.7}Sr_{0.3}MnO_3$ [16] in order to be able to compare results at different Sr doping.

The perovskite manganites have an ideal cubic structure ($Pm\bar{3}m$) above ~750 K [1]. With cooling $La_{1-x}Sr_xMnO_3$ acquires a rhombohedral structure ($R\bar{3}c$), as a result of a rotation of the MnO_6 octahedra around the [111] axis. $La_{0.8}Sr_{0.2}MnO_3$ shows another structural transition to a orthorhombic phase below $T \approx 120\,\text{K}$ [1]. However, it was shown that low-energy phonons, in particular acoustic modes, can still be well described by a cubic shell model [19]. Therefore, we use the cubic notation for all wave vectors. The wave vectors are given in reciprocal lattice units of $(2\pi/a, 2\pi/b, 2\pi/c)$, where $a = b = c = 3.86\,\text{Å}$.

III. RESULTS

We investigated $[1\bar{1}0]$-polarized TA phonons of $\sum_3$ symmetry dispersing in the [110] direction at various temperatures. The symmetry of $\sum_3$ phonons match the displacement pattern of the JT distortion of the MnO_6 octahedra and the COO of the CE type [19,20]. The latter is characterized by superlattice peaks at $\boldsymbol{q}_{\text{CE}} = (1/4, 1/4, 0)$, e.g., in $La_{0.7}Ca_{0.3}MnO_3$ [9] and $La_{1.2}Sr_{1.8}Mn_2O_7$ [21]. The structure factor of these TA phonons is large close to the reciprocal lattice vector $\boldsymbol{\tau} = (2,2,0)$, where measurements can be performed in a purely transverse geometry, i.e., $\boldsymbol{\tau} \perp \boldsymbol{q}$ in $\boldsymbol{Q} = \boldsymbol{\tau} + \boldsymbol{q} = (2, 2, 0) + (-h, +h, 0)$.

The neutron-scattering intensities at $\boldsymbol{Q} = (2-h, 2+h, 0)$ as a function of h are represented in color-coded contour plots shown in Figs. 1(a)–1(c). We observe sharp phonon peaks and a well-defined dispersion at low temperatures [Fig. 1(a)]. The TA phonon branch dominates the spectrum at $h \leqslant 0.3$. There is an anticrossing of the TA branch with a transverse optical (TO) branch near $h \approx 0.35$. Close to the zone boundary ($h \approx 0.45-0.5$) two well-separated phonons appear at 8.3 and 15.8 meV.

We studied the wave-vector and temperature dependence of the TA and TO modes by analyzing energy scans at constant-momentum transfer as shown in Figs. 1(d)–1(f). For $E \leqslant 5\,\text{meV}$ the experimental background for each temperature was obtained from the zone boundary scans. For $E \geqslant 12\,\text{meV}$ it was obtained from the zone center (not shown) and approximated by a straight line [dashed lines in Figs. 1(d)–1(f)] for the energies in between.

Energy scans at constant-momentum transfers were approximated with damped harmonic oscillator (DHO) functions convoluted with the calculated Gaussian resolution [Figs. 1(d)–1(f)]. The Bose factor built in to the DHO function accounts for the observed integrated intensities of the TA phonons at the zone boundary at increasing temperatures. The peak just above 10 meV is an artifact exhibiting no detectable temperature dependence. Hence, it was described by a

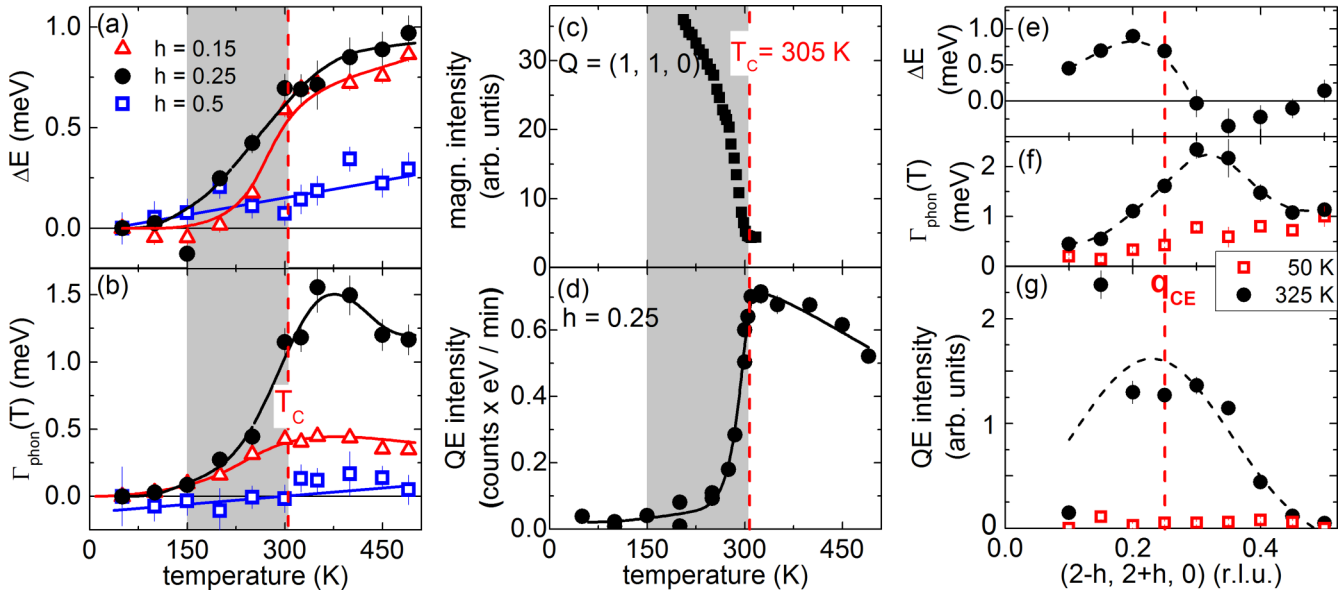

FIG. 2. (Left) Temperature dependences of (a) phonon softening ΔE and (b) phonon linewidth Γ_{phon} (HWHM) with respect to results obtained at $T = 50$ K data shown for $\boldsymbol{Q} = (2-h, 2+h, 0)$, $h = 0.15$, 0.25, and 0.5. (Middle) Temperature dependences of (c) the intensity of the (110) Bragg peak with a strong ferromagnetic contribution below the Curie temperature $T_C = 305$ K and (d) quasielastic scattering intensity at $h = 0.25$ extracted from raw data as shown in Figs. 1 and 3. Solid lines are guides to the eye. The temperature range characterized by anomalous phonon softening and broadening at $h = 0.15$ and 0.25 is marked in gray in panels (a)–(d). The upper end of the gray region coincides with the Curie temperature $T_C = 305$ K. (Right) Momentum dependences of phonon (e) softening ΔE, (f) linewidth Γ_{phon}, and (g) QE intensity at $T = 325$ K (dots) compared to results obtained at $T = 50$ K (open squares). Dashed lines are Gaussian fits to the data at $T = 325$ K over the indicated momentum ranges.

temperature-independent Gaussian function and posed no problem for further analysis [16]. Higher-energy TO phonons were fitted with simple Gaussians. A reduced phonon energy can be generally expected on heating because of thermal expansion and increasing thermal atomic motions. However, such a behavior should be similar for all phonon modes. The TA zone boundary phonon at $h = 0.5$ shows an energy reduction (softening) of 3% on heating from 150 to 325 K and its intensity increases according to the Bose factor. On the other hand, the TA mode at $h = 0.25$ softens by 0.81 meV, i.e., 9%, and acquires an intrinsic linewidth of 1.2 meV on heating from 150 to 325 K [Figs. 1(d)–1(f)]. Furthermore, the intensity increase between 250 K [Fig. 1(e)] and 325 K at low energies [Fig. 1(f)] cannot be explained alone by the TA phonon mode. Hence, we introduced a Lorentzian peak centered at $E = 0$ describing quasielastic (QE) scattering if the linewidth is not resolution limited.

Heating through $T_C = 305$ K leads to a pronounced low-energy tail of the TA phonon around $\boldsymbol{q}_{\text{CE}} = (1/4, 1/4, 0)$ [Fig. 1(c)]. Detailed temperature dependences of phonon softening (ΔE) and linewidth for $h = 0.15$, 0.25, and 0.5 are shown in Figs. 2(a) and 2(b). We find similarly strong softening at the two smaller wave vectors, whereas the broadening is strongest close to $h = 0.25$, which corresponds to the COO ordering wave vector $\boldsymbol{q}_{\text{CE}} = (1/4, 1/4, 0)$ observed in many FM manganites. Note that softening and broadening expected from thermal expansion and thermally induced disorder are considerably smaller as observed in the results for the zone boundary mode at $h = 0.5$ [Figs. 2(a) and 2(b)].

The anomalous softening and broadening extend up to about the Curie temperature of 305 K, which we determined from the temperature dependence of the (110) Bragg reflection [Fig. 2(c)]. At higher temperatures, further softening becomes consistent with thermal expansion effects also observed at $h = 0.5$. The intensity of the Lorentzian at $E = 0$ and $h = 0.25$ strongly increases within the same temperature range as the phonon renormalization and reaches a maximum close to T_C [Fig. 2(d)].

The momentum dependences observed at 325 K ($>T_C$) show clear maxima along the [110] direction [Figs. 2(e)–2(g)]. The maxima for the softening, broadening, and QE intensity are at $h = 0.19$, 0.3, and 0.23, respectively [see dashed lines in Figs. 2(e)–2(g)]. This behavior is similar but less pronounced in the sample with $x = 0.3$ [16]. The width in momentum space of QE scattering in $La_{1-x}Sr_xMnO_3$ with $x = 0.2$ seems to be slightly larger than for $x = 0.3$, giving a correlation length of $\xi_{x=0.2} = 28(6)$ Å vs $\xi_{x=0.3} = 34(4)$ Å. However, the difference depends entirely on the outlier at $h = 0.15$, which is possibly related to an artifact produced by the resolution function combined with the proximity to a strong Bragg peak for small h. Unfortunately, the scattering angle in the experiment limited further investigations at smaller energies.

Thus, our data reveal that phonon renormalization along with QE scattering intensity are strongest at T_C. [Figs. 2(e)–2(g)]. QE scattering intensity is strongest close to $\boldsymbol{q}_{\text{CE}}$ and the largest phonon softening and broadening are located just below and above this wave vector, respectively. Hence, we focus on the temperature dependences deduced from measurements at $\boldsymbol{q}_{\text{CE}}$ in the following.

As in our previous investigation of $La_{0.7}Sr_{0.3}MnO_3$ [16], we assign the strong QE Lorentzian scattering to dynamic polaron correlations of the CE type, which effectively trap the

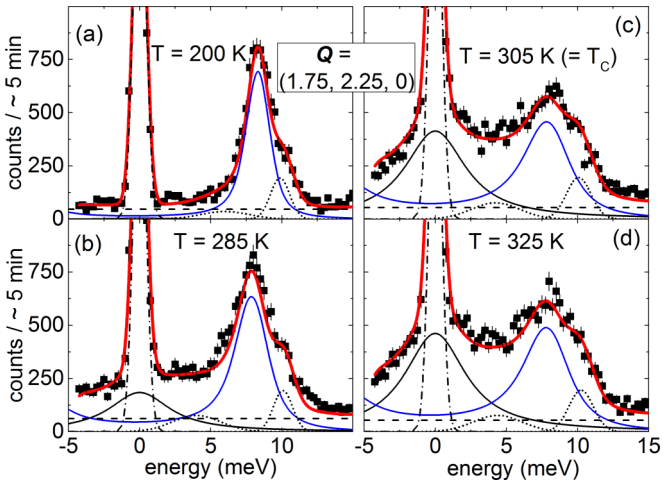

FIG. 3. Energy scans from −4 to 15 meV at $\boldsymbol{Q} = (1.75, 2.25, 0)$ for (a) $T = 200$, (b) 285, (c) 305, and (d) 325 K. Solid (red) lines are fits consisting of a damped harmonic oscillator function for the TA mode (solid and blue), a Lorentzian for QE scattering (solid and black), and the estimated background (dashed). The dotted lines denote temperature-independent artifacts (∼5 and 10 meV). The resolution-limited line at $E = 0$ (dashed-dotted line) is due to incoherent scattering and is practically temperature independent.

conduction electrons above T_C. However, the energy scans shown in Figs. 1(d)–1(f) were not adequate to determine the linewidth of the Lorentzian peak, i.e., the lifetime of the QE scattering. In order to determine both amplitude and linewidth of the Lorentzian at $h = 0.25$, we performed additional inelastic neutron scattering measurements for $La_{1-x}Sr_xMnO_3$ with $x = 0.2$ in a slightly different configuration of the instrument, which allowed energy transfers from −4 to +15 meV. In these scans, the QE peak, which strongly increases at T_C, appears beneath a resolution-limited and practically temperature-independent elastic line [Figs. 3(a)–3(d)].

After correcting for the experimental resolution, the average width of the approximated Lorentzians at $300\,K \leqslant T \leqslant 325$ is $\Gamma_{polaron} = (2.03 \pm 0.23)$ meV [half width at half maximum (HWHM)], which corresponds to the lifetime of the polaron correlations of $t = (2.04 \pm 0.23)$ ps. By the same procedure we obtain $\Gamma_{polaron} = (4.15 \pm 0.63)$ meV (HWHM) and $t = (1.0 \pm 0.15)$ ps at $325\,K \leqslant T \leqslant 400\,K$ for $La_{0.7}Sr_{0.3}MnO_3$ [16]. The temperature dependence of QE scattering linewidth and the deducted lifetime in $La_{1-x}Sr_xMnO_3$ for $x = 0.2, 0.3$ are given in Figs. 4(a) and 4(b). Although we detected the QE peak well below 300 K, its width could only be determined with high accuracy closely below and above T_C where the QE intensity is greatly enhanced. Uncertainty in the linewidth increases strongly on cooling well below T_C in both compounds, due to strongly decreasing QE scattering intensities.

QE scattering intensities at the two doping levels are harder to compare than peak positions and linewidths, because they depended on sample size. We employed the intensities of the TA phonon at $h = 0.25$ and $T = 200\,K$ measured in both compounds (Fig. 5) in order to calculate the scaling factor between the neutron-scattering data taken on the two samples.

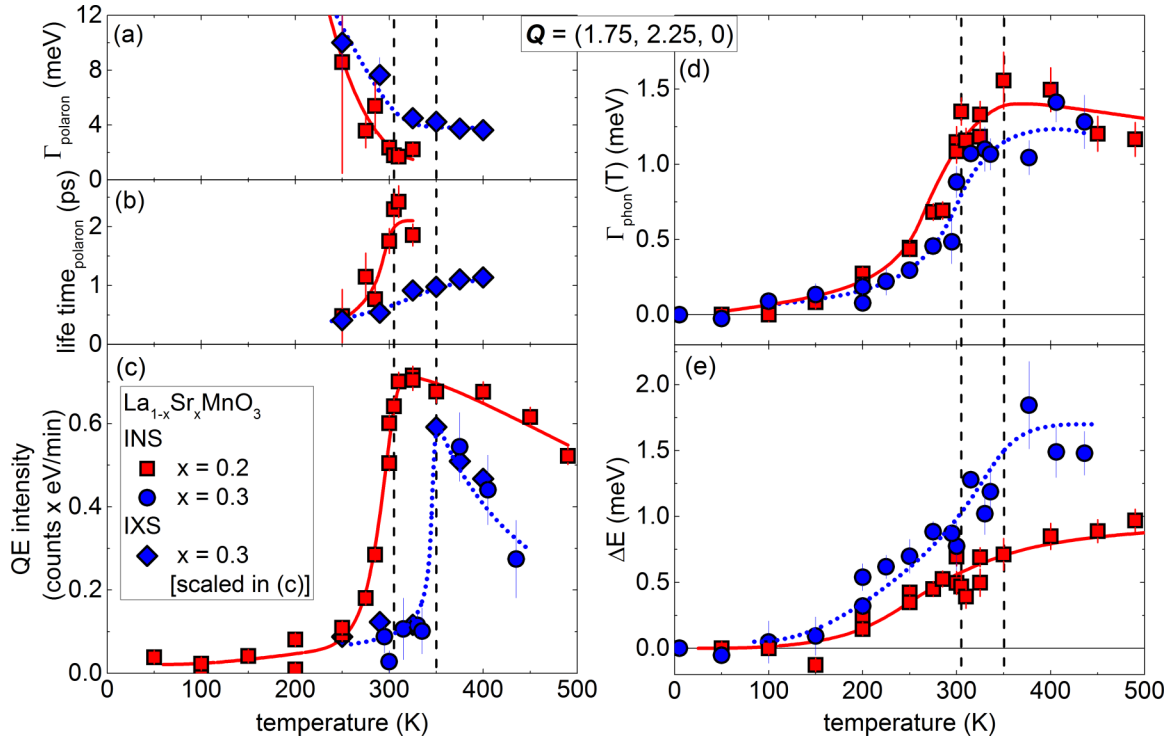

FIG. 4. QE scattering (left) and phonon renormalization (right) for $La_{1-x}Sr_xMnO_3$ ($x = 0.2, 0.3$) at $h = 0.25$. (a) Linewidth $\Gamma_{polaron}$, (b) lifetime, and (c) normalized intensity of QE scattering associated with CE polaronic correlations. (d) Phonon linewidth Γ_{phon} (HWHM) and (e) difference between the phonon energy at low temperature and just above T_C, ΔE. The intensities of the $x = 0.3$ data in (c) were normalized to $x = 0.2$ data by multiplication with a factor of 0.33 (see text and Fig. 5). Solid and dotted lines are guides to the eye. Vertical dashed lines represent $T_C = 305$ and 350 K for $x = 0.2, 0.3$. INS and IXS denote inelastic neutron scattering and inelastic x-ray scattering, respectively.

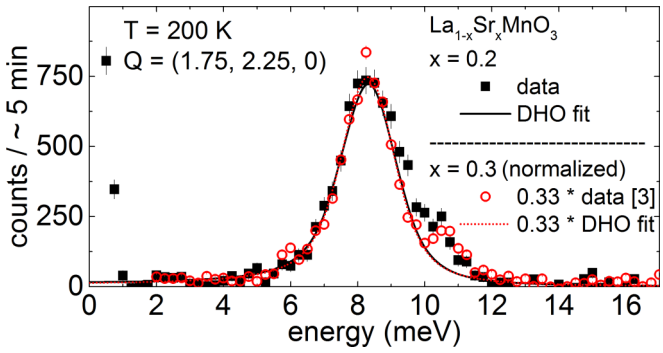

FIG. 5. (a) Energy scan (background subtracted) of the TA phonon at $\boldsymbol{Q} = (1.75, 2.25, 0)$ and $T = 200$ K for $La_{1-x}Sr_xMnO_3$ ($x = 0.2, 0.3$). The intensities of $x = 0.3$ data can be normalized to those of $x = 0.2$ data by multiplication with a factor of 0.33 obtained from the ratio of integrated intensities. The small peak at 10.5 meV is a temperature-independent artifact.

We determine it at 200 K because the influence of the QE scattering is still negligible and the background underneath the phonon is flat. The analysis in Fig. 5 shows that there is a factor of 0.33 difference in the absolute intensities in the two measurements, i.e., the scattering intensities obtained for the $La_{1-x}Sr_xMnO_3$ sample with $x = 0.3$ can be scaled to match those obtained for $x = 0.2$ if they are multiplied by 0.33 (Fig. 5).

Our comparison for the two different doping levels shows that QE scattering intensity is higher in the lower-doped sample featuring a larger CMR effect [Fig. 4(c)]. Yet, the average increase from $x = 0.3$ to $x = 0.2$ is about a factor of 1.5, i.e., smaller than the factor of 2 reported for the CMR strength (see Table I) [14]. In contrast, phonon broadening is the same [Fig. 4(d)] and the phonon softening is smaller [Fig. 4(e)] for the TA mode at $h = 0.25$ in $La_{0.8}Sr_{0.2}MnO_3$. Only the difference of the lifetimes of the polaronic correlations, 2.04(23) ps and 1.00(15) ps for $La_{0.8}Sr_{0.2}MnO_3$ and $La_{0.7}Sr_{0.3}MnO_3$, respectively [Fig. 4(b)], match the difference in the CMR strength.

IV. DISCUSSION

Table I summarizes our results together with available analogous results on other CMR manganites taken from literature. We clearly see that the increase of the CMR strength is correlated with a decreasing Curie temperature. However, it is the main result of our investigation that this increase of the CMR strength is, at least in the $La_{1-x}Sr_xMnO_3$ family, not related to a corresponding increase of EPC since the increase of the linewidths of the TA phonon across T_C are the same in $La_{0.7}Sr_{0.3}MnO_3$ and $La_{0.8}Sr_{0.2}MnO_3$. Instead, our results indicate that the strength of the CMR scales (within uncertainty) with polaron lifetime.

The polaronic lattice distortion magnitude, which determines the intensity of the quasielastic scattering in our data, can be expected to have a strong effect on the strength of the CMR. However, we show that it seems to be similar in $La_{0.8}Sr_{0.2}MnO_3$ compared to $La_{0.7}Sr_{0.3}MnO_3$. Furthermore, all available data indicate that these intensities are of the same order of magnitude [22], even including the bilayer manganite $La_{1.2}Sr_{1.8}Mn_2O_7$ [13,20] and $La_{0.7}Ca_{0.3}MnO_3$ [12], where CMR effects are up to two orders of magnitude stronger than in $La_{1-x}Sr_xMnO_3$.

Similarly, correlation lengths ξ of polarons are of the same order of magnitude for several CMR compounds listed in Table I, despite strongly varying strengths of the CMR effects. Therefore, it is unlikely that the correlation length is the driving factor for the CMR.

Incipient structural phase transitions involving short-range polaronic fluctuations tend to destabilize the atomic lattice, leading to softening of phonons resembling the CE-type charge and orbital order. If the lifetime of polaronic fluctuations increases, the lattice should stabilize into a new structure, which is expected to result in smaller phonon softening. We observe this behavior in $La_{1-x}Sr_xMnO_3$, where the $x = 0.2$ sample shows a larger polaron lifetime resulting in harder phonons, i.e., a smaller phonon softening compared to $x = 0.3$.

Strong phonon renormalization effects indicating QE fluctuations in the FM phase of $La_{1.2}Sr_{1.8}Mn_2O_7$ develop above T_C into the characteristic Jahn-Teller distortion with an elastic superlattice peak close to $\boldsymbol{q}_{CE}$ [20], where the CE-order is short-range and static. Another investigation of the bilayer manganite $La_{1.2}Sr_{1.8}Mn_2O_7$ by Ref. [21] shows that the linewidth of QE and elastic scattering slightly above T_C is resolution limited ($\approx$2 meV) and not measurable below T_C. However, the presence of an elastic superlattice peak in $La_{1.2}Sr_{1.8}Mn_2O_7$ indicates significantly larger lifetimes of the polarons compared to our results in $La_{1-x}Sr_xMnO_3$. Thus, a quantitative analysis of polaron lifetime below T_C is very desirable for further investigations into $La_{1.2}Sr_{1.8}Mn_2O_7$, due to its significantly larger CMR effect compared to $La_{1-x}Sr_xMnO_3$.

TABLE I. Curie temperatures, applied magnetic field, and corresponding magnetoresistance $\frac{-[\rho(B)-\rho(0)]}{\rho(0)}$ and drop of resistivity at T_C($\frac{\rho(B=0)}{\rho(B\neq 0)}$) polaron lifetime, and correlation length of some CMR compounds. The polaron lifetime measured in $La_{1-x}Ca_xMnO_3$ ($x = 0.2, 0.3$) is limited to 2 ps, set by the energy resolution of spectrometer [25].

Material	T_C (K)	B (T)	$\frac{-[\rho(B)-\rho(0)]}{\rho(0)}$	$\frac{\rho(0)}{\rho(B)}$ @ T_C	Pol. lifetime (ps)	Corr. length ξ (Å)	Reference
$La_{0.7}Sr_{0.3}MnO_3$	350	15	0.35	2	1.00(15)	34(4)	[14]
$La_{0.8}Sr_{0.2}MnO_3$	305	15	0.75	4	2(23)	28(6)	[14]
$La_{0.8}Ca_{0.2}MnO_3$	178				>2	14	[25]
$La_{0.75}Ca_{0.25}MnO_3$	245	4	0.84	6			[12]
$La_{0.7}Ca_{0.3}MnO_3$	227	5	0.97	30	>2	28	[23,25]
$La_{1.2}Sr_{1.8}Mn_2O_7$	118	14	0.99	300		16	[20]

Another example resembling the behavior described before is observed in the 50% doped bilayer manganite $LaSr_2Mn_2O_7$, which however has an insulating low-temperature ground state exhibiting a long-range charge and orbital CE order [24] with no metal-insulator transition. This polaronic ground state is comparable to the high-temperature insulating phase above T_C in $La_{1-x}Sr_xMnO_3$ ($x = 0.2, 0.3$) or $La_{1.2}Sr_{1.8}Mn_2O_7$. The difference compared to, e.g., $La_{1-x}Sr_xMnO_3$ ($x = 0.2, 0.3$) is that the half-doped $LaSr_2Mn_2O_7$ shows a "perfect" ordering of Mn^{3+} (JT-active) and Mn^{4+} (JT-inactive) ions leading to a static polaronic lattice with an "infinite" lifetime. Within the COO state the transverse acoustic phonon at $\boldsymbol{q}_{CE}$ (see Fig. 3(b) in Ref. [24]) shows no renormalization effects in agreement with our proposition, i.e., that an infinite lifetime of the polaronic correlations results in a very small or absent phonon renormalization.

In comparison to $La_{1-x}Sr_xMnO_3$ and in respect to CMR strength (Table I), we expect polaron lifetimes that are one order of magnitude ($\approx$10 ps) larger in $La_{1-x}Ca_xMnO_3$ (0.2−0.3) and two orders of magnitude ($\approx$100 ps) larger in the bilayer manganite $La_{1.2}Sr_{1.8}Mn_2O_7$. A detailed comparative high-energy-resolution study of phonons, intensities, and lifetimes of polaronic correlations in, e.g., the bilayer manganite $La_{2-x}Sr_{1+2x}Mn_2O_7$ and the $La_{1-x}Ca_xMnO_3$ series would be highly desirable in order to investigate these relations over a larger range in the strength of the CMR effect.

V. CONCLUSION

We report inelastic neutron-scattering data revealing dynamic polaronic correlations of CE type in $La_{0.8}Sr_{0.2}MnO_3$ similar to our previous findings in higher-doped $La_{0.7}Sr_{0.3}MnO_3$ [16]. Strong renormalization of the TA phonons propagating along the [110] is associated with the polaronic behavior. A quantitative comparison of phonons and polarons in $La_{1-x}Sr_xMnO_3$, $x = 0.2$ and 0.3, shows that lifetime and intensity of polaronic correlations scale with the strength of CMR but phonon renormalization and other properties, e.g., polaronic correlation length, do not. This study needs to be extended to compounds with larger CMR (see Table I) in order to test the proposed correlation between the CMR strength and the lifetime of polaronic correlations in FM manganites.

ACKNOWLEDGMENTS

M.M. and F.W. were supported by the Helmholtz Society under the Contract No. VH-NG-840. D.R. was supported by the DOE, Office of Basic Energy Sciences, Office of Science, under Contract No. DE-SC0006939.

[1] Y. Tokura, Rep. Prog. Phys. **69**, 797 (2006).
[2] R. von Helmolt, J. Wecker, B. Holzapfel, L. Schultz, and K. Samwer, Phys. Rev. Lett. **71**, 2331 (1993).
[3] S. Jin, T. H. Tiefel, M. Mccormack, R. A. Fastnacht, R. Ramesh, and L. H. Chen, Science **264**, 413 (1994).
[4] H. A. Jahn and E. Teller, Proc. R. Soc. London, Ser. A **161**, 220 (1937).
[5] A. J. Millis, P. B. Littlewood, and B. I. Shraiman, Phys. Rev. Lett. **74**, 5144 (1995).
[6] A. J. Millis, B. I. Shraiman, and R. Mueller, Phys. Rev. Lett. **77**, 175 (1996).
[7] D. M. Edwards, Adv. Phys. **51**, 1259 (2002).
[8] P. G. Radaelli, D. E. Cox, M. Marezio, and S. W. Cheong, Phys. Rev. B **55**, 3015 (1997).
[9] C. P. Adams, J. W. Lynn, Y. M. Mukovskii, A. A. Arsenov, and D. A. Shulyatev, Phys. Rev. Lett. **85**, 3954 (2000).
[10] J. B. Goodenough, Phys. Rev. **100**, 564 (1955).
[11] E. O. Wollan, Phys. Rev. **100**, 545 (1955).
[12] P. Schiffer, A. P. Ramirez, W. Bao, and S. W. Cheong, Phys. Rev. Lett. **75**, 3336 (1995).
[13] X. J. Chen, C. L. Zhang, C. C. Almasan, J. S. Gardner, and J. L. Sarrao, Phys. Rev. B **67**, 094426 (2003).
[14] A. Urushibara, Y. Moritomo, T. Arima, A. Asamitsu, G. Kido, and Y. Tokura, Phys. Rev. B **51**, 14103 (1995).
[15] Y. Tokura, A. Urushibara, Y. Moritomo, T. Arima, A. Asamitsu, G. Kido, and N. Furukawa, J. Phys. Soc. Jpn. **63**, 3931 (1994).
[16] M. Maschek, D. Lamago, J. P. Castellan, A. Bosak, D. Reznik, and F. Weber, Phys. Rev. B **93**, 045112 (2016).
[17] Q. Li, K. E. Gray, H. Zheng, H. Claus, S. Rosenkranz, S. Nyborg Ancona, R. Osborn, J. F. Mitchell, Y. Chen, and J. W. Lynn, Phys. Rev. Lett. **98**, 167201 (2007).
[18] RESCAL: http://www.ill.eu/instruments-support/computing-for-science/cs-software/all-software/matlab-ill/rescal-for-matlab/.
[19] W. Reichardt and M. Braden, Physica B **263**, 416 (1999).
[20] F. Weber, N. Aliouane, H. Zheng, J. F. Mitchell, D. N. Argyriou, and D. Reznik, Nat. Mater. **8**, 798 (2009).
[21] D. N. Argyriou, J. W. Lynn, R. Osborn, B. Campbell, J. F. Mitchell, U. Ruett, H. N. Bordallo, A. Wildes, and C. D. Ling, Phys. Rev. Lett. **89**, 036401 (2002).
[22] F. Weber, D. N. Argyriou, O. Prokhnenko, and D. Reznik, Phys. Rev. B **88**, 241106 (2013).
[23] C. S. Hong, W. S. Kim, and N. H. Hur, Solid State Commun. **121**, 657 (2002).
[24] F. Weber, S. Rosenkranz, J.-P. Castellan, R. Osborn, H. Zheng, J. F. Mitchell, Y. Chen, S. Chi, J. W. Lynn, and D. Reznik, Phys. Rev. Lett. **107**, 207202 (2011).
[25] P. C. Dai, J. A. Fernandez-Baca, N. Wakabayashi, E. W. Plummer, Y. Tomioka, and Y. Tokura, Phys. Rev. Lett. **85**, 2553 (2000).